IOPscience iopscience.iop.org

Home Search Collections Journals About Contact us My IOPscience

Crystalline multilayers of charged colloids in soft confinement: experiment versus theory

This article has been downloaded from IOPscience. Please scroll down to see the full text article.

2012 J. Phys.: Condens. Matter 24 464123

(http://iopscience.iop.org/0953-8984/24/46/464123)

View the table of contents for this issue, or go to the journal homepage for more

Download details:
IP Address: 134.99.64.185
The article was downloaded on 02/11/2012 at 08:50

Please note that terms and conditions apply.

J. Phys.: Condens. Matter **24** (2012) 464123 (9pp) doi:10.1088/0953-8984/24/46/464123

Crystalline multilayers of charged colloids in soft confinement: experiment versus theory

E C Oğuz[1], A Reinmüller[2], H J Schöpe[2], T Palberg[2], R Messina[1,3] and H Löwen[1]

[1] Institut für Theoretische Physik II, Heinrich-Heine-Universität Düsseldorf, Universitätsstraße 1, 40225 Düsseldorf, Germany
[2] Institut für Physik, Johannes Gutenberg-Universität Mainz, Staudingerweg 7, 55128 Mainz, Germany
[3] Institut de Chimie, Physique et Matériaux (ICPM), Université de Lorraine, 1 Bld Arago, 57078 Metz-Cedex 3, France

E-mail: ecoguz@thphy.uni-duesseldorf.de

Received 26 March 2012, in final form 27 March 2012
Published 31 October 2012
Online at stacks.iop.org/JPhysCM/24/464123

Abstract
We combine real-space experiments and lattice sum calculations to investigate the phase diagram of charged colloidal particles under soft confinement. In the experiments we explore the equilibrium phase diagram of charged colloidal spheres in aqueous suspensions confined between two parallel charged walls at low background salt concentrations. Motivated by the experiments, we perform lattice sum minimizations to predict the crystalline ground state of point-like Yukawa particles which are exposed to a soft confining wall potential. In the multilayered crystalline regime, we obtain good agreement between the experimental and numerical findings: upon increasing the density we recover the sequence $2\square \rightarrow 2\triangle \rightarrow 2\text{hcp}\perp \rightarrow 3\square \rightarrow 3\triangle \rightarrow 3\text{hcp}\perp \rightarrow 4\square$.

(Some figures may appear in colour only in the online journal)

1. Introduction

The behavior of particles in confinement can be drastically different from that found in the bulk [1]. In particular, phase transitions like crystallization are strongly shifted or even changed in nature for strong confinement [2–4]. The type of confinement can be either topographical ('hard') or energetic ('soft'). The former case is typically modeled by hard system boundaries which influence the local packing or imprint a local substrate structure onto the system. One of the standard situations is confinement in a slit geometry between two parallel hard plates. Soft confinement, on the other hand, results from a smooth external potential, a typical situation of which is particles confined in a harmonic well. The nature of confinement needs to be distinguished from the interactions between the particles which can also be hard (as, e.g., for hard spheres) or soft (as given for, e.g., Yukawa-like pair interactions).

Colloidal suspensions have been used as model systems for various types of interaction and confinement [5] thanks to the tunability of their interactions [6] and the susceptibility of the particles to external fields. Sterically stabilized colloids represent a realization of a hard-sphere system, while charged colloids are mainly described by Yukawa pair interactions [7–9]. Likewise hard and soft slit-geometry confinement can be realized by constraining the suspensions between plates. Uncharged plates provide a hard confinement while a large surface charge leads to long-ranged repulsions resulting in a soft confinement. One big advantage of colloidal systems is that individual particle positions are observable directly (e.g. by video microscopy)[4] providing real-space access to crystallization phenomena [11–15]. An understanding of crystallization phenomena in quasi-two-dimensional system

[4] Scattering provides an alternative method in Fourier space, see, e.g., [10].

 © 2012 IOP Publishing Ltd Printed in the UK & the USA

is important not only for a fundamental understanding but also for applications like optical filters [16] and micro-sieves [17].

Regarding crystallization in slit geometry, hard confinement has been studied for both hard particles [11, 18–28] and soft particles [12, 29–38]. More recently, the case of hard particles in soft confinement has also been addressed, see, e.g., [39, 40]. Complex cascades of multilayered crystals were predicted and confirmed in colloidal experiments the details of which depend on the interparticle and particle–wall interactions. Detailed comparisons between experiment and theory were performed for hard [11, 24, 26] and soft [12] particles in hard confinement but for soft particles in soft confinement such a direct comparison is missing.

In this paper, we close this gap and compare the crystallization of soft particles in soft confinement, by both theory and experiment. In the experiments, charged colloidal spheres in a highly deionized solvent are confined between two charged glass plates. In theory, we consider point-like Yukawa interactions between the particles, thereby interpolating between two known extreme limits of unscreened Coulomb particles [33, 41, 42] and hard spheres [40] in soft confinement. Focusing on multicrystalline layering, we combine both real-space studies of charged suspensions and lattice sum calculations of a Yukawa model at zero temperature in soft confinement. The comparison between the experimental data and a DLVO-type model for the interparticle and particle–wall interactions performs quantitatively well within the given uncertainties. In particular, we confirm the basic multilayer phase sequence $2\square \to 2\triangle \to 2\text{hcp}\perp \to 3\square \to 3\triangle \to 3\text{hcp}\perp \to 4\square$ if the system density increases.

This paper is organized as follows. In section 2, we discuss the experiments and present real-space data for multilayered crystals. The lattice sum calculations are briefly explained and the resulting ground state phase diagrams are compared to the experimental findings in sections 3 and 4. We finish with concluding remarks in section 5.

2. Experiments

2.1. Principles

We experimentally explored the equilibrium phase diagram of charged colloidal spheres in aqueous suspensions under spatial confinement in slit geometry at low background salt concentrations using a home-made setup. The suspensions were prepared in a closed tube system [43] including the microscopy cell, a mixed bed ion exchanger column and a syringe pump. The ion concentration was monitored using an integrated conductivity measurement cell. The arrangement of components in a circuit facilitated efficiently deionizing and homogenizing the suspensions via pumping. The measurement cell consisted of optically flat quartz substrates attached to piezo actuators for adjusting the confining geometry. The confined volume between the circular substrates had a lateral diameter of 25 mm and was in contact with the surrounding bulk volume. A proper choice of materials of high ionic purity as well as carefully sealing the whole setup guaranteed sufficiently low contamination with salt ions. Optionally the whole setup could be enclosed into a glove bag providing a nitrogen atmosphere. The conditions were reasonably stable for more than 20 min each time after stopping the pump. Observations were made using a conventional inverted optical scientific microscope (Leica, DM-IRB, Germany). Two mono-disperse aqueous suspensions of negatively charged polystyrene spheres with diameters $2a_1 = (5.19 \pm 0.08)\ \mu$m and $2a_2 = (2.59 \pm 0.04)\ \mu$m (batch nos PS/Q-F-B1036 and PS-F-B233 by Micro Particles Berlin GmbH, Germany; in the following these will be termed 'PS 5.2 μm' and 'PS 2.6 μm') were used. In order to suppress gravity the solvent mass density was matched to that of polystyrene by adding 20 vol% glycerol. Prior to the measurements the stock suspensions were in contact with mixed bed ion exchange resins for several weeks.

At constant chemical properties of both particle and substrate surfaces we investigated the equilibrium phase diagram in terms of the emerging crystal structures depending on the dimensionless parameters, namely the reduced area number density η and the reduced inverse screening length λ:

$$\eta = n_\text{A} d^2 = n_\text{P} d^3, \tag{1}$$

$$\lambda = \kappa d. \tag{2}$$

Herein n_A and n_P denote the area and volume particle number density respectively, d is the width of the confining slit and κ is the inverse screening length of the assumed repulsive, screened Coulomb interparticle potential. In our experiments these parameters could be varied and determined quantitatively.

The area number density $n_\text{A} = N/A$ was evaluated by counting the number N of particles observed in the specified field of view A of an optical micrograph showing a well-defined phase. Counting was performed in a partly automated way by using image analysis algorithms[5].

The separation d between the confining walls was *in situ* accessible via white light interferometry. To that end the quartz substrates were specifically coated with a beam splitting gold layer (10 nm gold on 1.5 nm chromium on quartz; optical transmission ca. 50%; sputtering was performed by the Max Planck Institute for Polymer Research, Mainz, Germany). To induce a negative wall charge in contact with aqueous suspensions further coatings were produced in a dip procedure [44]: first the gold layer was coated with a cysteamine monolayer (cysteamine hydrochloride by Sigma-Aldrich) that chemically bonded via a thiol group and provided a positive surface charge. Subsequently a sodium polystyrene sulfonate coating (poly(sodium 4-styrenesulfonate) by Sigma-Aldrich) was produced. The latter polymeric layer provided a negative surface charge and bonded electrostatically to the cationic cysteamine layer. At wall separations below $d \leq 50\ \mu$m and at sufficiently low area number densities n_A, i.e. when the observed area A was not completely covered with particles but

[5] For example, by use of ImageJ (open source program currently available under http://rsbweb.nih.gov/ij/).

there were free interstices visible between the particles, the transmitted spectrum of a white light illumination (e.g. the microscopy lamp) showed pronounced interference peaks and dips typical for Fabry–Pérot resonators. These interference patterns allowed quantitative evaluation of the local wall separation according to

$$d = \frac{c}{2n_r \Delta f} = \frac{1}{2n_r(\lambda_i^{-1} - \lambda_{i+1}^{-1})}, \tag{3}$$

where n_r denotes the refractive index of the suspension, Δf the frequency shift between two succeeding interference peaks and λ_i and λ_{i+1} the corresponding optical wave lengths.

Taking into account the particle counter ions and additional monovalent salt ions in the suspensions the bulk inverse screening length reads [43]

$$\kappa = \sqrt{\frac{e^2}{\epsilon\epsilon_0 k_B T}(Z^* n_P + 2000 N_A c_S + 2000 N_A 10^{-7}\ \mathrm{mol\,l^{-1}})}, \tag{4}$$

where e is the elementary charge, $\epsilon\epsilon_0$ is the electrical permittivity, $k_B T$ is the thermal energy, N_A is Avogadro's number, c_S is the salt concentration (in mol l^{-1}) and Z^* is a parameter representing an effective particle charge. The third term within the brackets describes the contribution due to autoprotolysis of water. The quantities c_S and Z^* were gathered from bulk conductivity measurements. The total conductivity σ reads [45]

$$\sigma = n_P e Z^*(\mu_{H^+} + \mu_P) + 1000 N_A c_S e(\mu_{salt,+} + \mu_{salt,-}) + \sigma_{H_2O}, \tag{5}$$

where the first term on the right hand side describes the contribution of particles and particle counter ions, the second term describes the salt contribution and $\sigma_{H_2O} = 0.055\ \mu S\ cm^{-1}$ (at 25 °C) is the conductivity background due to autoprotolysis of water. We assume only contamination with airborne CO_2 so that in this particular case the salt cations and particle counter ions are both H^+. Otherwise, the complete formula by Hessinger *et al* [45] would have to be used. The quantities $\mu_{H^+} = 36.2 \times 10^{-8}\ m^2\ V^{-1}\ s^{-1}$ (in pure water at 25 °C), μ_P, $\mu_{salt,+}$ and $\mu_{salt,-}$ are the ionic mobilities of hydrogen cations, particles, salt cations and salt anions respectively. We can identify $\mu_{salt,+} \approx \mu_{H^+}$ and $\mu_{salt,-} \approx \mu_{HCO_3^-}$ ($= 4.6 \times 10^{-8}\ m^2\ V^{-1}\ s^{-1}$ in pure water at 25 °C).

Laser Doppler velocimetry measurements [46] of the electrophoretic particle mobilities of the PS 5.2 μm particles revealed values in the range of $\mu_P = 3.3 \times 10^{-8}\ m^2\ V^{-1}\ s^{-1} \approx 0.1\mu_{H^+}$ for highly diluted suspensions in pure water under CO_2-saturated conditions. However, the glycerol within the suspension is expected to affect especially the mobilities $\mu_{HCO_3^-}$ and μ_P, which are assumed to depend inversely on the solution's viscosity. We therefore multiplied both $\mu_{HCO_3^-}$ and μ_P by a factor of 0.56 taken from the literature [47]. The parameter Z^* could be estimated from the bulk conductivity σ_0 of the totally desalinated suspensions, i.e. when $c_S = 0$, under which conditions equation (5) simplifies to

$$\sigma_0 = n_P e Z^*(\mu_{H^+} + \mu_P) + \sigma_{H_2O}. \tag{6}$$

Under the assumption of generally small particle mobilities, $\mu_P \approx 0.05\ \mu_{H^+}$, equation (6) yields

$$Z^* \approx \frac{\sigma_0 - \sigma_{H_2O}}{1.1\mu_{H^+} n_P e}. \tag{7}$$

At increased salt concentrations then by combining equations (5) and (6) it follows that

$$c_S = \frac{\sigma - \sigma_0}{1000 N_A e(\mu_{salt,+} + \mu_{salt,-})}. \tag{8}$$

2.2. Observations

We performed several measurement series exploring crystalline phases at salt concentrations between $c_S \approx 0.02$ and $0.3\ \mu mol\ l^{-1}$ and at volume fractions in the confined volume between $\phi \approx 8\%$ and 10.5% for the larger PS 5.2 μm particles and between $\phi \approx 2.4\%$ and 3.6% for the smaller PS 2.6 μm particles. The experiments were made at room temperature. After stopping the pump and adjusting the confining geometry both optical micrographs and transmission spectra from the local field of view were recorded at different wall separations or at different spatial positions. The wall separation was varied in a range between $d \approx 10$ and 30 μm. Sudden changes of d induced strong fluid currents that shear melted the existing colloidal structures. Re-formation of colloidal structures occurred within typically 1 min. Measurements were usually performed during time periods of less than 20 min before deionizing and homogenizing the suspension was started again. Within this time period the conductivity typically increased by $\Delta\sigma \leq 0.05\ \mu S\ cm^{-1}$ which corresponds to an increase of salt concentration of $\Delta c_S \leq 0.15\ \mu mol\ l^{-1}$.

In the chosen range of parameters we reproducibly observe crystalline but also a fluid phase for both species of particles. Typical in-plane nearest neighbor distances were $d_{NN} \approx 9\ \mu$m for the larger PS 5.2 μm particles and $d_{NN} \approx 6.5\ \mu$m for the smaller PS 2.6 μm particles. Phase diagrams indicating the measured crystalline data points are shown in figure 1, while additional diagrams displaying also fluid data points are given in figure 2. A selection of optical micrographs showing exemplary crystalline structures for both species of particles is given in figures 3 and 4.

We clearly observe a sequence of crystalline structures depending on the parameters λ and η (cf figure 1). Basically layered structures of triangular symmetry ($n\triangle$) and square symmetry ($n\square$) alternate with increasing d:

$$\cdots \to n\triangle \to (n+1)\square \to (n+1)\triangle \to \cdots, \tag{9}$$

where n denotes the number of layers. The structures $n\triangle$ correspond to fcc-(111) or hcp-(001) faces aligned parallel to the confining walls, while the structures $n\square$ correspond to fcc-(100) faces respectively.

Different transition structures are superimposed on the basic sequence according to equation (9). First, the buckling transition [19, 20] B was frequently observed. More or less pronounced line buckling occurred, but no unconventional types of buckling [48] were evident. Secondly, structures of vertically aligned triangular layers ($n$hcp$\perp$) [23] equivalent

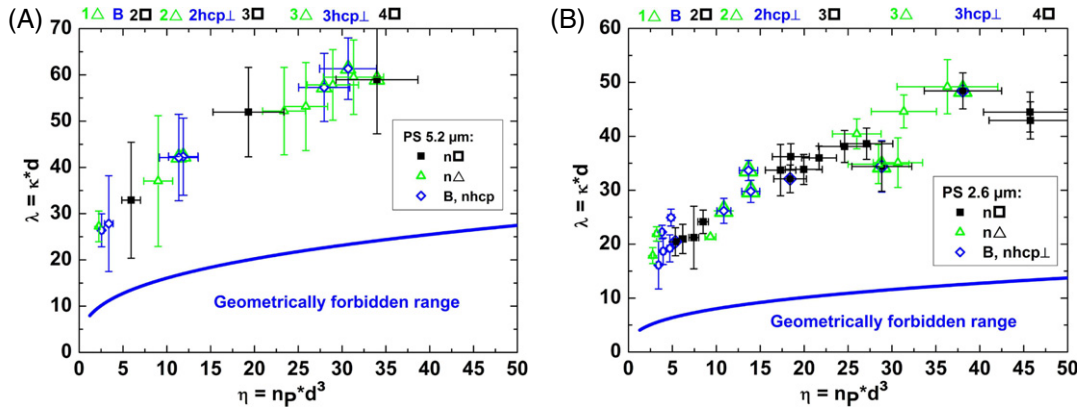

Figure 1. Experimentally observed crystalline equilibrium phases of charged colloidal spheres in slit confinement. ((A) PS 5.2 μm; (B) PS 2.6 μm; the symbols in the diagram label the data points.) See main text for further information.

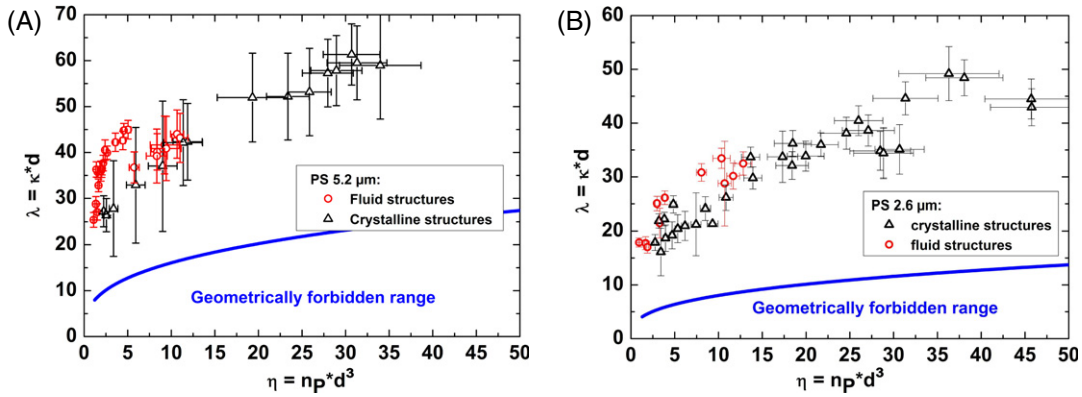

Figure 2. Selected data points corresponding to fluid structures (red circles) and crystalline structures (black triangles) ((A) PS 5.2 μm; (B) PS 2.6 μm).

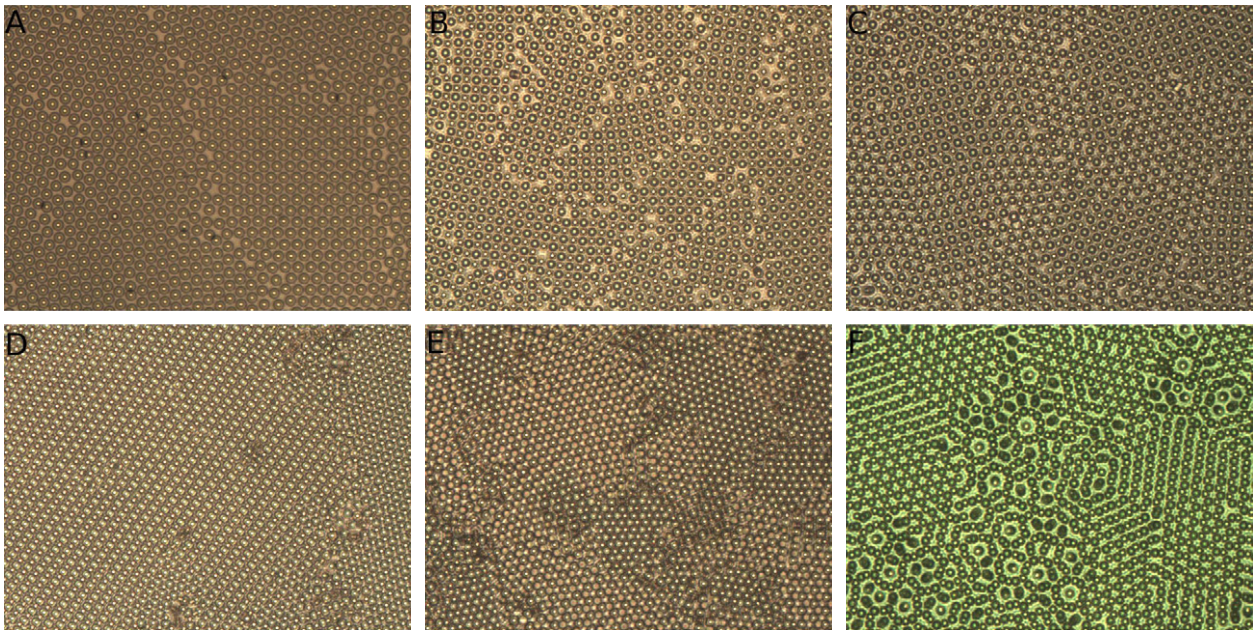

Figure 3. Examples of crystalline structures observed in our experiments with the larger PS 5.2 μm particles: 1△ (A), 2□ (B), coexistence of 2□ and 2△ (C), 2hcp⊥ (central large domain) in coexistence with 2△ (grain at the right margin) (D), 3△ with different appearances of fcc(111) and hcp(001) faces (E) and moiré rosettes in coexistence with 2hcp⊥ and 2△ (F). (Field of view: 280 × 210 μm^2.)

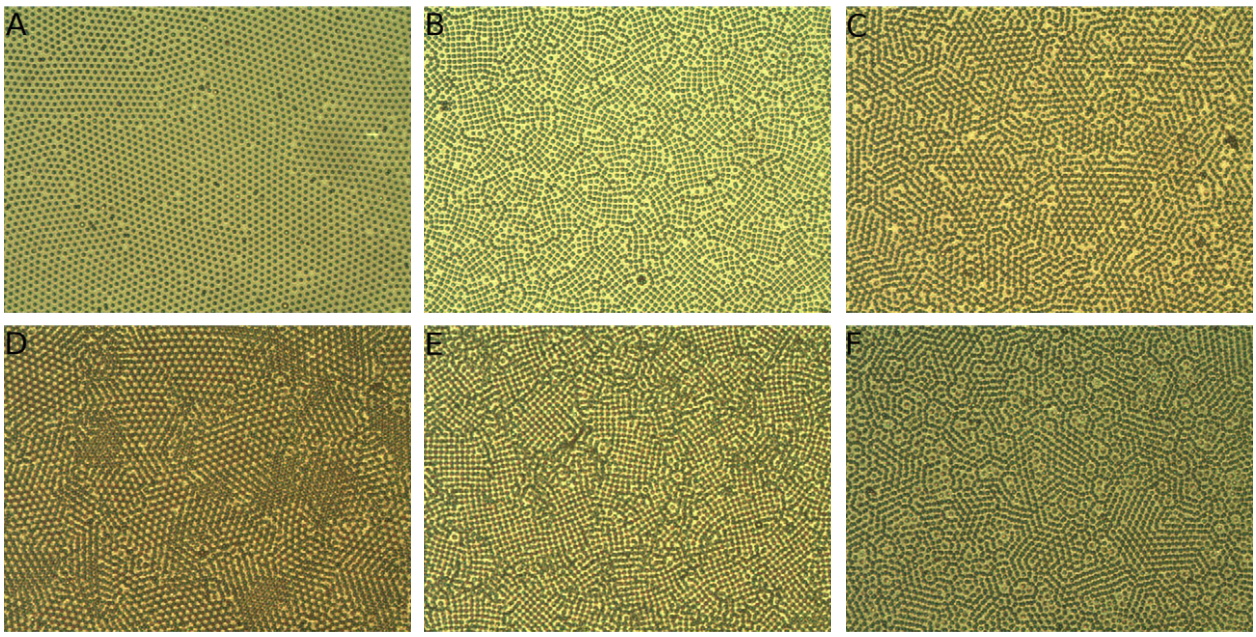

Figure 4. Examples of crystalline structures observed in our experiments with the smaller PS 2.6 μm particles: 1△ (A), 2□ (B), 2△ (C), 3△ with different appearances of fcc(111) and hcp(001) faces (D), 4□ (E) and moiré rosettes in coexistence with 2hcp⊥ and 2△ (F). (Field of view: 350 × 265 μm^2.)

to hcp-(110) faces were observed. Further, coexisting with 2△ and 2hcp⊥ some specific structures featuring pronounced rosette-shaped particle arrangements were observed. These have recently been identified as meta-stable moiré rotation patterns consisting of two unconventionally stacked triangular monolayers [35]. These structures formally correspond to $1 \times 1R\alpha$ superstructures, where α denotes discrete rotation angles. In summary, the whole observed experimental sequence reads (without the transient moiré patterns)

$$1\triangle \rightarrow B \rightarrow 2\square \rightarrow 2\triangle \rightarrow 2\text{hcp}\perp \rightarrow 3\square \rightarrow 3\triangle \rightarrow 3\text{hcp}\perp \rightarrow 4\square. \quad (10)$$

The range containing the observed crystalline phases is bordered by a geometrically forbidden range, where the particle number densities exceed the maximum packing limit, and the region of fluid structures (cf figure 2). The borderline (blue lines) of the geometrically forbidden range was estimated assuming a constant maximum volume fraction of $\phi = 60\%$ in the confining slit and a minimum total ion concentration $c = 2\times10^{-7}$ mol l^{-1} neglecting particle counter ions and salt ions. Reasonably, fluid structures were observed at larger λ, i.e. at weaker particle interactions, with respect to crystalline structures.

Fluid structures in the regime of more than two layers as well as crystalline phases with more than four layers were not evaluated quantitatively. Too large area number densities n_A did not allow measurements of the wall separation d nor of the locally observed particle numbers N due to too many visually overlapping particles. Further, particle fluctuations made structures more difficult to identify, and sufficiently large crystalline grains did not form within a reasonable time period.

The formation of monolayer and bilayer crystals typically occurred quasi-instantaneously within 10 s, while systems with more layers required longer times to emerge. On timescales of about 5 min slow changes of morphology were observed that did not affect the crystalline structures. Defects were annealed and grain boundaries slowly vanished by diffusive particle rearrangement. Further long-term relaxation processes of the system were observed on timescales of 20 min. A slow decrease of the local particle number density n_P in the confined suspension occurred which induced an increase of crystal lattice constants and even led to melting of crystalline structures. This temporary loss of particles during measurements is presumably due to a difference between the chemical potentials of confined and bulk suspensions. This was the main obstacle to long time measurements. The original values n_P could afterwards be restored via homogenizing.

Major error sources in our experiments are inexact particle counting, weak interferometric contrast in estimating d, salt contaminations and thermal effects. The former two are considerable, especially for more than two particle layers, when many particles are visually overlapping due to the large particle diameter $2a$ with respect to their typical distance $d_{NN} \approx 1.5 - 2.5 \times 2a$. Salt contaminations are always present and more significant for lower overall salt concentrations. Further uncertainty arises from the fact that the conductivity could not be measured *in situ*, but only apart from the confinement cell in bulk. Local ion sources, like, e.g., tiny fragments of ion exchange resins [49], cannot generally be excluded. But it is also not *a priori* clear how wall counter ions affect the local ion concentration and thus the local interparticle interactions. This might give rise to systematic errors that were not further considered. Thermal effects,

e.g. induced by the microscopy illumination, might appear as local thermal gradients. Thermogradients may influence the particle concentrations by thermophoresis. Of more interest probably would be local changes of the particle interaction. The dependence is complex but can be assumed small [50]. Carefully estimated error bars are indicated in figures 1 and 2.

3. Theory

3.1. The model

We consider N point-like particles interacting via a Yukawa pair potential

$$V(r) = V_0 \frac{\exp(-\kappa r)}{\kappa r}, \tag{11}$$

where r is the interparticle distance and V_0 denotes the energy amplitude. For charged suspensions, this interaction amplitude is given within DLVO theory [51, 52] as

$$V_0 = \frac{Z^{*2} e^2 \kappa}{4\pi\epsilon_0\epsilon} \left(\frac{\exp(\kappa a)}{1+\kappa a}\right)^2, \tag{12}$$

where a denotes the physical hard-core radius of the particles and ϵ is the dielectric permittivity of the solvent. We further invoke linear screening theory to describe the wall–particle interaction by the confining potential [53]

$$V_c(z) = W_0 \cosh(\kappa z), \tag{13}$$

with z denoting the direction perpendicular to the plates. The amplitude W_0 is given by (see e.g. [7, 31, 53–55])

$$W_0 = \frac{2Z^* e^2}{\epsilon_0\epsilon} \sigma_w \frac{\exp(\kappa a)}{\kappa(1+\kappa a)} \exp(-\lambda/2). \tag{14}$$

Using the interaction potentials above, we performed lattice sum minimizations to obtain the stability phase diagram at zero temperature, as explained and discussed in the following.

3.2. Lattice sum minimization

We performed lattice sum minimizations for a broad set of candidates of crystalline lattices. Here, we focus on the nontrivial multilayer regime beyond the stability of the squared bilayer 2□ phase. For fixed λ, a sufficient increase of the reduced density yields the squared tetralayer structure 4□. The precise goal of our work is to figure out the corresponding regime between 2□ and 4□ by investigating the stability of intervening crystalline multilayers.

For our lattice sum minimization problem the possible candidates are three-dimensional crystals with two-dimensional periodicity in the x- and y-directions and a finite extension in the z-direction. The primitive cell of these candidates is a parallelepiped containing k particles and its xy-basis (which is a parallelogram) is spanned by the two lattice vectors $\mathbf{a} = a(1, 0)$ and $\mathbf{b} = a\gamma(\cos\theta, \sin\theta)$, where γ is the aspect ratio ($\gamma = |\mathbf{b}|/|\mathbf{a}| = b/a$) and θ is the angle between $\mathbf{a}$ and $\mathbf{b}$. Furthermore, the k particles are distributed, not necessarily evenly, on n layers in the xy-plane. Here we restrict ourselves to layered situations with an up–down inversion symmetry in the averaged occupancy reflecting the up–down symmetry of the confining external field. Under this restriction, we consider possible candidates with $k = 2, \ldots, 6$ and $n = 1, \ldots, 6$ (up to symmetric six-layer structures with a basis of up to six particles). At prescribed system parameters, the total potential energy per particle is minimized with respect to the particle coordinates of the cell and its geometry (γ and θ).

3.3. Matching the model parameters to the experiments

This paper aims at a direct comparison between the theoretical results and the experimental ones so that a quantitative analysis naturally requires the knowledge of the two intrinsic energy scales V_0 and W_0 of the system. Hence, the phase behavior depends not only on the system density but also on the ratio W_0/V_0. Therefore we introduce the surface charge ratio $\nu = \sigma_w/\sigma_p = \sigma_w/(Z^*/4\pi a^2)$ ($\nu > 0$) between the wall and the spheres. In order to implement experimental conditions in our lattice sum calculations, we need to consider the following parameters: $Z^*, \epsilon, \kappa, a, \nu, d, n_P, T$. In fact, the effective charge Z^* of the colloid–colloid interaction as well as the solvent permittivity ϵ scale out at zero temperature ($T = 0$) for the colloids. Hence, at prescribed $\lambda = \kappa d$ and $\eta = n_P d^3$ the only relevant parameters are κ, a and ν.

Our primary goal is to predict the theoretical phase diagrams for large ($a = 2.6$ μm) and small ($a = 1.3$ μm) particles. Thereby with $\kappa \approx 1.5$–3.0 μm^{-1} we use averaged values of κ resulting in $\kappa a = 6$ ($\kappa a = 3$) for PS 5.2 μm (PS 2.6 μm) particles.

Next we estimate the surface charge ratio ν which enters into the particle–wall interaction (14). One has to keep in mind that, although the bare wall surface charge density is pretty high, the colloidal particles feel the wall only at large distances where most of the wall charge has been nonlinearly screened and the linear-screening-regime has been reached. Actually what enters into equation (14) is not the bare surface charge density but an effective surface charge density [7]. The latter can be brought into relation to the bare charge density via the exact Gouy–Chapman solution of the nonlinear Poisson–Boltzmann equation as worked out by von Grünberg and coworkers [56]. Using the procedure described in [56] a strong reduction of the bare wall charge to an effective wall charge is achieved.

In detail, the bare wall charge density can be estimated by the assumption that the polyelectrolytes form a dense monolayer on the walls with a molecular area density of $\sim 1/\pi r_g^2$, where the radius of gyration r_g is taken to be that in the concentrated solution used at coating. Under experimental conditions, the polyelectrolyte molecules will stretch to yield a bare charge density of the order of the molecular density. For the experimentally used polyelectrolyte coating we therefore estimate the real charge density of the walls as $(4 \pm 1) \times 10^{-3}$ nm^{-2}. Following the procedure given in [56], the effective wall charge density is reduced towards 0.7–1.2 × 10^{-3} nm^{-2}. On the other hand, the effective surface charge density on the colloidal spheres is typically about 2.4 ×

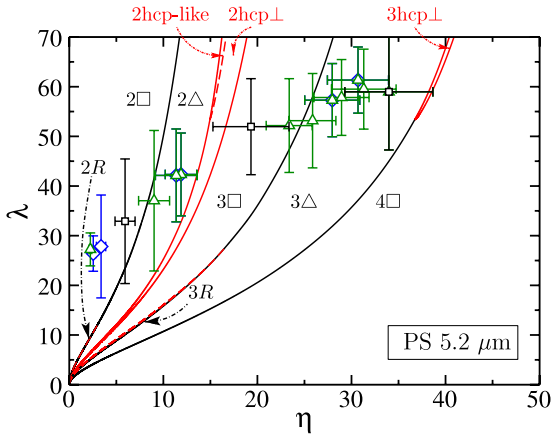

Figure 5. Comparison of the theoretical prediction (dashed and full lines) for the multilayer stability phase diagram at zero temperature to the experimental data (symbols) taken from the phase diagram for PS 5.2 μm particles in figure 1(A). Here, we use $\kappa a = 6$ and $v = 0.4$. Please note that symbols for the experimental data are as in figure 1. See main text for further information.

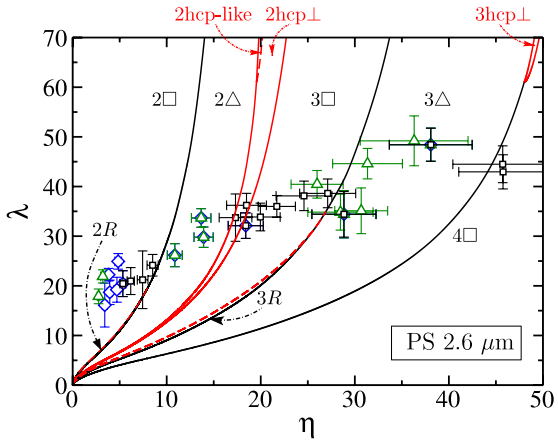

Figure 6. The same as figure 5 for PS 2.6 μm particles (with $\kappa a = 3$ and $v = 0.4$).

10^{-3} nm^{-2} (2.0×10^{-3} nm^{-2}) for 5.2 μm (2.6 μm) particles such that v becomes roughly $0.3 \leq v \leq 0.5$ ($0.4 \leq v \leq 0.6$) for 5.2 μm (2.6 μm) particles. In the following we have chosen $v = 0.4$, which leads to a good agreement between theory and experiments. Moreover, as our theoretical analysis shows, a different choice of v in the range $0.1 < v < 0.5$ does not significantly change the theoretical data such that the comparison is fortunately quite insensitive to the actual choice of v.

3.4. Ground state phase diagrams and comparison to experiments

At zero temperature, for a given reduced density η, the system will minimize its total potential energy, and the resulting optimal ground state structure will solely depend on the reduced inverse screening length $\lambda = \kappa d$. Under consideration of the system at hand, the calculations have been performed for 5.2 and 2.6 μm particles and the corresponding phase diagrams are drawn in figures 5 and 6.

We explore the stability phase diagram for $0 < \lambda \leq 70$ and $0 < \eta \leq 50$ and we investigate the structural transitions between the phases 2□ and 4□. Thereby, we obtain several multilayered crystalline phases with rhombic (R), triangular (△), quadratic (□) and rectangular (hcp-like, hcp⊥) symmetry. In the transition regime 2□ → 4□ there are not only bilayered (2R, 2△) and trilayered (3□, 3R, 3△) phases evident, we further even notice the stability of tetralayered (2hcp-like, 2hcp⊥) as well as a hexalayered (3hcp⊥) phase.

Both the rhombic phases 2R and 3R display tiny stability regimes, which are indicated by the red dashed lines in figures 5 and 6 and which vanish above a certain threshold of λ. The phases hcp-like, hcp⊥ and 3hcp⊥, which become stable for $\lambda \gtrsim 51.9$ ($\lambda \gtrsim 59.6$) for PS 5.2 μm (PS 2.6 μm) particles, are derivable from the hcp lattice as recently discussed in [21, 23]. We further remark that the stacking sequence of 3R (3△) consists of the *ABA* (*ABC*) one. In all resulting structures the size ratio of the lattice vectors equals unity ($\gamma = 1$) except for 2hcp-like, 2hcp⊥ and 3hcp⊥. In this case, γ is larger than 1 due to its rectangular basis shape.

Clearly, for relatively small λ, the phase diagram reveals the following phase cascade interpolating between 2□ and 4□:

$$2\square \to 2\mathrm{R} \to 2\triangle \to 2\mathrm{hcp}\perp \to 3\square \to 3\mathrm{R} \to 3\triangle \to 4\square. \quad (15)$$

However, for relatively large reduced inverse screening length we notice the stability of the rhombic phases 2R and 3R to vanish and the stability of 2hcp-like and 3hcp⊥ to arise yielding the following stability sequence:

$$2\square \to 2\triangle \to 2\mathrm{hcp\text{-}like} \to 2\mathrm{hcp}\perp \to 3\square \to 3\triangle \to 3\mathrm{hcp}\perp \to 4\square. \quad (16)$$

Regarding the order of the transitions, both first- and second-order transitions occur and are indicated by solid and dashed transition lines in figures 5 and 6, respectively. The second-order transitions are $n\square \to n\mathrm{R}$ for $n = 2, 3$ and 2hcp-like → 2hcp⊥, whereas all remaining transitions exhibit discontinuous paths in at least one of the order parameters θ and/or γ.

4. Discussion

The charged walls in the experiments lead to a soft exponentially screened wall–particle interaction which we implicitly considered by the effective external field given by equation (12) in our theoretical model. However, we did not take the hard-core part of the walls into account explicitly there. This can be justified by the wall charge density which was high enough to keep particles well separated from the walls and prevent sticking to them. Besides, as the experiments are realized in the low screening regime, the particles are not touching each other so that the pair potential from equation (11) without explicit hard-core interaction is reasonable for the effective colloid–colloid interaction.

We achieve a good quantitative agreement between the theoretical and experimental phase diagrams (cf figures 5 and 6). The stability domains of the experimentally found phase structures coincide well with the corresponding phase boundaries obtained by lattice sum calculations. However, the stability domains of the $n$hcp$\perp$ phases might be slightly off the theoretically predicted ones (especially for large particles and 3hcp$\perp$).

The phase diagrams for both the PS 5.2 μm and the PS 2.6 μm particles (cf figures 1(A) and (B)) are in qualitative agreement, but they do not match quantitatively. For the larger particles the fluid region is located at significantly larger values of λ at given η, while the crystalline structures are also shifted to smaller values of η. These discrepancies might be attributed to the experimental non-zero particle size.

Comparing our results with those from similar experiments performed previously by van Winkle and Murray [57] shows qualitative agreement in the basic sequence of crystal structures with increasing d (cf equation (9)) together with the buckling transition B. However, the particle interactions were not specified there. Their phase diagram is rather determined by geometric parameters only.

Comparison of our experimental results under strongly deionized conditions with those from wedge confinement experiments in the strongly screened limit [12, 18] also shows agreement in the basic sequence (cf equation (9)) together with the transition phases B and $n$hcp$\perp$. But here we do not observe crystalline prism phases [11, 24] (nP), nor do we have clear evidence of rhombic phases [19, 20, 33] (nR). Theory [32] suggests that prism phases are predominantly stable in strongly screened suspensions, but not at weak screening as it is the case here. In fact, prism phases have frequently been observed experimentally in the strongly screened limit [11, 12]. The prism phases apparently possess more particles in the outer layers than in the inner ones [11, 24, 32]. Since the outer particles cause energy loss due to the external field, absence of the prism phases is not surprising. Even for higher densities η, we expect the multilayering scenario to favor phases that have more or comparable weights in the inner layers than in the outer ones.

Theory further predicts that rhombic phases should especially occur in the transitions

$$n\square \rightarrow n\mathrm{R} \rightarrow n\triangle \tag{17}$$

for $n = 2$–4 [33]. The absence of clear evidence of rhombic phases in the experiments might be explained by ground state stability arguments (cf the theoretical phase diagrams in figures 5 and 6): the stability domains of 2R and 3R are too tiny. In these transition regions we rather observe coexisting $n\square$ and $n\triangle$ structures in the experiments. Interestingly, $n = 2$ crystallites of $2\square$ and $2\triangle$ favor commensurate instead of disordered grain boundaries (cf figure 3(C)). Hence, lattice distortions occur in order to reduce the grain boundary energy, which give rise to regions of rhombically ordered particles. But it remains unclear whether these are equilibrium structures or morphologically induced, meta-stable structures. Further discrepancies between the experimental phase diagrams (figures 1, 2) and theoretical ground state phase diagrams (figures 5, 6) might be attributed to finite temperature effects.

5. Conclusions

In conclusion, we have compared real-space data for the crystallization of charged colloids in soft confinement with zero-temperature lattice sum calculations of a Yukawa system in a soft wall potential as predicted by linear screening theory. We found quantitative agreement and have confirmed the basic multilayer phase sequence

$$2\square \rightarrow 2\triangle \rightarrow 2\mathrm{hcp}\perp \rightarrow 3\square \rightarrow 3\triangle \rightarrow 3\mathrm{hcp}\perp \rightarrow 4\square$$

as the system density increases. As one of the essential input parameters, the quantitative comparison needed the surface charge density ratio ν of the walls and the particles. This ratio was chosen to be smaller than unity implying that the walls are effectively less charged than the colloidal particles. The good comparison shows that the linearized theory is applicable to confined charged colloids and that most of the physics is contained in an effective pairwise potential model with soft interactions.

We further obtained first- and second-order phase transitions in the ground state phase diagrams (figures 5 and 6) which are shown by solid and dashed transition lines in figures 5 and 6, respectively.

In future work, more subtle effects should be considered on the theoretical side which could improve the comparison. Possibilities include a finite excluded-volume core of the colloids, finite temperature of the particles [58], charge polydispersity of the suspensions [59], as well as image charges resulting from the jump in the dielectric permittivity from the aqueous solution to the wall [55]. On the experimental side, to overcome the above described restrictions of small accessible layer numbers and small accessible ranges of n_P, new experiments can be performed with suspensions providing $d_\mathrm{NN}/2a \gg 2$, e.g. using suspensions of comparably interacting, but smaller particles. Also confocal microscopy can be used to provide a better three-dimensional structure analysis in similar experiments.

We expect further interesting new physics of a multicrystalline layer that is sheared. Shear flow would promote alignment effects and could lead to novel reentrant behavior [58, 60–63]. It would further be interesting to study a patterned or curved wall which would introduce a new length scale to the confined crystalline layer leading to novel elastic response of the crystalline sheet as pointed out in various recent investigations [64–66].

Acknowledgments

We gratefully acknowledge financial support by the Deutsche Forschungsgemeinschaft (SFB-TR6 project D1, Pa459/15-17, Scho1054/3). We further acknowledge technical support by Holger Schweinfurth, Institut für Physik, Universität Mainz, Germany, and by the group of Dr G Auernhammer at Max Planck Institute for Polymer Research, Mainz, Germany.

References

[1] Drake J M and Klafter J 1990 *Phys. Today* **43** 46
[2] Dietrich S and Haase A 1995 *Phys. Rep.* **260** 1
[3] Alba-Simionesco C *et al* 2006 *J. Phys.: Condens. Matter* **18** R15
[4] Löwen H, Oğuz E C, Assoud L and Messina R 2012 *Adv. Chem. Phys.* **148** 225
[5] Löwen H 2001 *J. Phys.: Condens. Matter* **13** R412
[6] Yethiraj A 2007 *Soft Matter* **3** 1099
[7] Hansen J-P and Löwen H 2000 *Ann. Rev. Phys. Chem.* **51** 209
[8] Löwen H and Allahyarov E 1998 *J. Phys.: Condens. Matter* **10** 4147
[9] Allahyarov E, D'Amico I and Löwen H 1999 *Phys. Rev.* E **60** 3199
[10] Satapathy D K *et al* 2009 *Europhys. Lett.* **87** 34001
[11] Neser S, Bechinger C, Leiderer P and Palberg T 1997 *Phys. Rev. Lett.* **79** 2348
[12] Fontecha A B *et al* 2005 *J. Phys.: Condens. Matter* **17** S2779
[13] Peng Y *et al* 2010 *Phys. Rev. Lett.* **104** 205703
[14] Peng Y *et al* 2011 *Phys. Rev.* E **83** 011404
[15] For a review, see Löwen H 2010 *Soft Matter* **6** 3133
[16] Park H S and Xia Y 1999 *Langmuir* **15** 266
[17] Goedel W A and Yan F 2004 *Nano Lett.* **4** 1193
[18] Pieranski P, Strzelecki L and Pansu B 1983 *Phys. Rev. Lett.* **50** 900
[19] Schmidt M and Löwen H 1996 *Phys. Rev. Lett.* **76** 4552
[20] Schmidt M and Löwen H 1997 *Phys. Rev.* E **55** 7228
[21] Ramiro-Manzano F, Bonet E, Rodriguez I and Meseguer F 2007 *Phys. Rev.* E **76** 050401
[22] Pickett G T, Gross M and Okuyama H 2000 *Phys. Rev. Lett.* **85** 3652
[23] Fontecha A B, Palberg T and Schöpe H J 2007 *Phys. Rev.* E **76** 050402
[24] Fortini A and Dijkstra M 2006 *J. Phys.: Condens. Matter* **18** 371
[25] Eral H B, van den Ende D, Mugele F and Duits M H G 2009 *Phys. Rev.* E **80** 061403
[26] Ramiro-Manzano F, Bonet E, Rodriguez I and Meseguer F 2009 *Soft Matter* **5** 4279
[27] Eral H B *et al* 2010 *Langmuir* **26** 16722
[28] Eral H B, Mugele F and G D H 2011 *Langmuir* **27** 12297
[29] Messina R and Löwen H 2003 *Phys. Rev. Lett.* **91** 146101
[30] Grandner S and Klapp S H L 2008 *J. Chem. Phys.* **129** 244703
[31] Löwen H *et al* 2008 *J. Phys.: Condens. Matter* **20** 404221
[32] Oğuz E C, Messina R and Löwen H 2009 *Europhys Lett.* **86** 28002
[33] Oğuz E C, Messina R and Löwen H 2009 *J. Phys.: Condens. Matter* **21** 424110
[34] Grandner S and Klapp S H L 2010 *Europhys. Lett.* **90** 68004
[35] Reinmüller A, Schöpe H J and Palberg T 2010 *Soft Matter* **6** 5312
[36] Oğuz E C, Messina R and Löwen H 2011 *Europhys Lett.* **94** 28005
[37] Kahn M, Weis J-J and Kahl G 2010 *J. Chem. Phys.* **133** 224504
[38] Kaneko T, Mima T and Yasuoka K 2010 *Chem. Phys. Lett.* **490** 165
[39] Deb D *et al* 2011 *J. Chem. Phys.* **134** 214706
[40] Curk T *et al* 2012 *Phys. Rev.* E **85** 021502
[41] Goldoni G and Peeters F M 1996 *Phys. Rev.* B **53** 4591
[42] Piacente G, Hai G Q and Peeters F M 2010 *Phys. Rev.* B **81** 024108
[43] Evers M, Garbow N, Hessinger D and Palberg T 1998 *Phys. Rev.* E **57** 6774
[44] Patricio S *et al* 2010 *Langmuir* **26** 10842
[45] Hessinger D, Evers M and Palberg T 2000 *Phys. Rev.* E **61** 5493
[46] Medebach M, Shapran L and Palberg T 2007 *Colloids Surf.* B **56** 210
[47] Lide D R and Frederikse H P R 1994 *Handbook of Chemistry and Physics* (Amsterdam: Elsevier)
[48] Chou T and Nelson D R 1993 *Phys. Rev.* E **48** 4611
[49] Reinmüller A *et al* 2012 *J. Chem. Phys.* **136** 164505
[50] Medebach M *et al* 2005 *J. Chem. Phys.* **123** 104903
[51] Hansen J-P and MacDonald I R 1948 *Theory of Stability of Lyophobic Colloids* (Amsterdam: Elsevier)
[52] Derjaguin B V and Landau L 1941 *Acta Physicochim. (USSR)* **14** 633
[53] Andelman D 1995 *Handbook of Biological Physics* ed R Lipowsky and E Sackmann (Amsterdam: Elsevier)
[54] Squires T M and Brenner M P 2000 *Phys. Rev. Lett.* **85** 4976
[55] Messina R 2009 *J. Phys.: Condens. Matter* **21** 113102
[56] von Grünberg H H, Helden L, Leiderer P and Bechinger C 2001 *J. Chem. Phys.* **114** 10094
[57] van Winkle D H and Murray C A 1986 *Phys. Rev.* A **34** 562
[58] Messina R and Löwen H 2006 *Phys. Rev.* E **73** 011405
[59] Löwen H, Roux J N and Hansen J P 1991 *J. Phys.: Condens. Matter* **3** 997
[60] Wu Y L, Derks D, van Blaaderen A and Imhof A 2009 *Proc. Natl Acad. Sci. USA* **106** 10564
[61] Shereda L T, Larson R G and Solomon M J 2010 *Phys. Rev. Lett.* **105** 228302
[62] Villanova-Vidal E, Palberg T, Schöpe H-J and Löwen H 2009 *Phil. Mag.* **89** 1695
[63] Stipp A *et al* 2004 *J. Phys.: Condens. Matter* **16** S3885
[64] Franzrahe K *et al* 2008 *J. Phys.: Condens. Matter* **20** 404218
[65] Franzrahe K, Nielaba P and Sengupta S 2010 *Phys. Rev.* E **82** 016112
[66] Irvine W T M, Vitelli V and Chaikin P M 2010 *Nature* **468** 947